Neural Computing and Applications (2019) 31:8411–8422
https://doi.org/10.1007/s00521-019-04528-8

ORIGINAL ARTICLE

Comparison of adaptive neuro-fuzzy inference system and recurrent neural network in vertical total electron content forecasting

Dinibel Pérez Bello[1,2] · María P. Natali[1,2] · Amalia Meza[1,2]

Received: 26 June 2019 / Accepted: 3 October 2019 / Published online: 21 October 2019

Abstract
Accurate prediction of total electron content (TEC) is important for monitoring the behavior of the ionosphere and indeed a magnitude of interest to understand the properties and behavior of the Sun–Earth System. The conditions of this medium have a direct impact on a growing variety of critical technological infrastructure. This work presents a comparison between two different artificial neural networks (ANNs): an adaptive neuro-fuzzy inference system and nonlinear autoregressive neural network (NAR-NN) applied to TEC. Both ANNs where tested on four different geomagnetic locations on 4 1-week periods having a variety of geomagnetic disturbance levels. The effect of using different training period lengths and the system response for 60 and 30 min sampling rate TEC time series was investigated. NAR-NN shows a slightly better performance, being the higher difference during the greater perturbations. There is also a better response when sampling rates of 30 min are used.

Keywords vTEC · Space weather · Neural network · Forecasting

1 Introduction

The term space weather (SW) has come into a great international scientific and public awareness today. It can be understood as the state of the Earth's atmosphere and the surrounding space as a result of their coupled response to the electromagnetic and particle emissions of the Sun and other cosmic sources on interplanetary space. SW's importance can be readily seen as the conditions of Earth's magnetosphere, thermosphere and ionosphere affect the performance and reliability of a number of key space- and ground-based technological systems, and beyond that, life and health [1].

As a consequence, there is a growing worldwide consensus on the need of practical tools for SW forecasting [1]. In fact, in 2015, the Committee on Space Research (COSPAR) of the International Council for Science (ICSU) and the International Living With a Star (ILWS) Steering Committee established a road map which identifies understanding the space environment as a high-priority challenge; pointing out the relevance of studying the geospace response to variable solar-wind stresses that lead to intense geomagnetically induced currents and ionospheric and radiation storm [2].

Thus, it is widely accepted that a key factor in forecasting SW is to model the state of the Earth's upper atmosphere. In particular, there are some parameters related to the ionosphere, i.e., the electron density (*NmF*2) or the critical frequency (*foF*2), the F layer peak height (*hmF*2) (or the propagation factor of the ratio of the maximum usable frequency at a distance of 3000 km to the F2 layer critical frequency (M(3000)F2) and the total electron content (TEC) [3]. The spatial and temporal coverage of *f*0*F*2 measurements is a relevant constraint. Different is the situation of TEC measurements that have a 24

✉ Dinibel Pérez Bello
dbello@fcaglp.unlp.edu.ar

María P. Natali
paula@fcaglp.unlp.edu.ar

Amalia Meza
amalia@fcaglp.unlp.edu.ar

[1] Consejo Nacional de Investigaciones Científicas y Técnicas (CONICET), Buenos Aires, Argentina

[2] Laboratorio de Meteorología espacial, Atmósfera terrestre, Geodesia, Geodinámica, diseño de Instrumental y Astrometría (MAGGIA), Universidad Nacional de La Plata, La Plata, Argentina

Table 1 Geomagnetic coordinates of the stations

Stations	Geomag. lat.	Geomag. long.
TUCU	17.19 S	7.12 E
LPGS	25.44 S	13.54 E
RIO2	44.06 S	4.20 E
OHI2	53.83 S	11.37 E

× 365 worldwide coverage thanks to the continuous International GNSS service (IGS) Global Navigation Satellite Systems (GNSS) tracking infrastructure implemented by the International Association of Geodesy (IAG).

Therefore, TEC became a significant parameter for scientific studies of structure and dynamics of the ionospheric plasma; consequently it has great importance for many applications. For instance, the TEC modeling can enhance the positioning accuracy of a GNSS [4, 5] and the monitoring of space weather events. Hence, TEC is an important parameter to detect ionospheric disturbances which could affect aircraft and spacecraft crew and equipment, wired and wireless communication, electric power distribution grids, surveying and navigation, all with a social and economical severe impact [6, 7].

Since the establishment of the IGS tracking infrastructure, GNSS became a well established tool for ionospheric sounding as these systems offer an unprecedented combination of accuracy, temporal and spatial resolution and availability. This led to important progress in fields such as ionospheric tomography [8] and the production of reliable global vertical total electron content (vTEC) maps in a continuous operational way in the context of the IGS [9–11]. With the regionally enormous increase in highly precise GNSS data, the demands on (near) real-time ionosphere products, necessary in many applications such as navigation, are growing very fast. Consequently, many analysis centers accepted the responsibility of generating such products. Some advances in this direction are the proposals by [12–15]. One step beyond are the products for ionospheric state forecasting. Attempts to generate reliable forecasting are described by [16].

Artificial neural networks (ANNs) have been found suitable for modeling phenomena exhibiting a high degree of nonlinearity in many scientific fields. Many authors have used different ANNs to predict ionospheric parameters, such as the critical frequency of the F2 layer of the ionosphere ($f0F2$), F2 layer peak electron density ($NmF2$) and vTEC. [17] showed the first application of ANNs to the prediction of $foF2$ using an input data indices of season (related with the day number), solar activity and magnetic activity; Wintoft and Cander [18] predicted the values of $foF2$ at Slough station for 24 h ahead under quiet and disturbed conditions, separately; using an input data solar and geomagnetic indices. Tulunay [19] developed the Middle East Technical University Neural Network (METU-NN) model to predict TEC; this model forecasts TEC values over Europe for 1 h and 10 min in advance using as input data the present values of vTEC, first, second and relative differences, the day of the year and the daily variation with a sine and cosine function. Tebabal [20] develop a local TEC model and forecasting using NN for two stations at low- and mid-latitude, taking into account solar and geomagnetic activity, time of the day and day of the year. Mallika [21] presents a forecasting algorithm based on the fusion of principal component analysis and artificial neural networks (PCA–NN) methods to forecast the ionospheric TEC values. The algorithm proposed as NN input's the PCA components of the TEC, solar flux and geomagnetic index, in addition to other necessary inputs for forecasting. This forecast was performed over a grid point in Japan using a 20-year period.

This work proposes the implementation of two neural networks for the prediction of vTEC under different geomagnetic conditions: an adaptive neuro-fuzzy inference system (ANFIS) and a model derived by a dynamic neural network based on the concept of a nonlinear autoregressive model (NAR-NN). The predicted vTEC value is based on a continuous learning process, allowing to have a predicted value at different time intervals, i.e., 1 h or 30 min. To achieve this objective, the training data are redefined for each instant to be predicted by entering new observed data

Table 2 Periods and characteristics of the geomagnetic storms used in the analysis

Period	Forecasting period		Storm start time		Minimum DST time	Minimum DST
		DOY	UT	LT	LT	
P1	09–15 Feb 2017	40–46	–	–	2017-02-10 04:00	− 15
P2	23–29 Mar 2017	82–88	2017-03-27 09:00	2017-03-27 06:00	2017-03-27 11:00	− 74
P3	24–30 May 2017	144–150	2017-05-27 21:00	2017-05-27 18:00	2017-05-28 04:00	− 125
P4	05–11 Sept 2017	248–254	2017-09-07 21:00	2017-09-07 18:00	2017-09-07 22:00	− 142
			2017-09-08 12:00	2017-09-08 09:00	2017-09-08 14:00	− 124

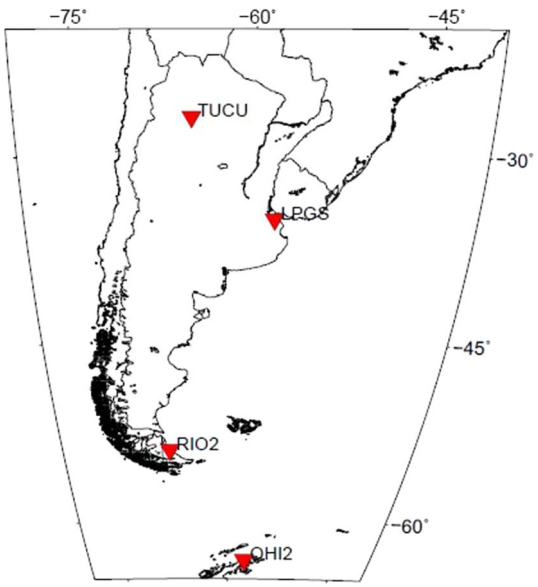

Fig. 1 Geographical distribution of the implemented stations

that are calculated by the different centers mentioned above.

This paper is organized as follow: in Sect. 2, we describe the data and the NNs applied in this work. Section 3 presents the results over four 1-week periods under different geomagnetic scenarios, and finally, in Sect. 4, the conclusions and the future work are presented.

2 Data and methodology

2.1 Data

Four different locations were selected to analyze the scope of the models: TUCU (Tucumán) near the equatorial anomaly, LPGS (La Plata) and RIO2 (Río Grande) for mid-latitudes and OHI2 (O'Higgins) for high latitude. See Table 1 and the map in Fig. 1.

The vTEC Global Ionopheric Maps (GIMs) are derived from GNSS dual-frequency measurements collected from the global IGS GNSS tracking network by the Center for Orbit Determination in Europe (CODE), the European Space Agency (ESA), the Jet Propulsion Laboratory (JPL) and the Universitat Politecnica de Catalunya (UPC) using different modeling techniques. In particular, UPC interpolates its two-layer tomographically calibrated vTEC estimation into 2-h resolution spline-based (UPRG), and 15 min kriging-based GIMs (UQRG) [22]. In this work, UQRG products were used to analyze the forecast model quality. Henceforth, the vTEC product of UQRG will be called $\mathrm{vTEC_{GNSS}}$. All datasets here mentioned are available in NASAs Archive of Space Geodesy Data at ftp://cddis.gsfc.nasa.gov/pub/gps/products/ionex/yyyy/ddd/.

The disturbance storm time (DST) index of hourly resolution, Fig. 2, was chosen as indicator of geomagnetic activity [37]. Based on this index, four 1-week periods, P1, P2, P3 and P4 (Table 2), were selected to test the forecasting capability of our models. Table 2 summarizes the Storm Start Time (in Universal Time, UT and Local Time, LT), the Minimum DST Time (in LT) and its corresponding Minimum DST as is published in the Space Weather Database Of Notifications, Knowledge, Information (DONKI) at https://kauai.ccmc.gsfc.nasa.gov/DONKI/.

Period P1 corresponds to a quiet week with minimum DST of − 15. P2 week includes a moderate geomagnetic activity characterized by a minimum DST of − 74. Periods P3 and P4 are highly perturbed, P3 with minimum DST of − 125, and P4 has two main disturbances, one with a minimum DST of − 142 and the other with a minimum DST of − 124. Figure 2 also included highlighting quiet and disturbed period behavior. In the following, we will compare the performance of our models in these different ionospheric conditions. The DST data were obtained from the GSFC/SPDF OMNIWeb interface at https://omniweb.gsfc.nasa.gov.

2.2 Input data

Given the time series $\mathrm{vTEC_{GNSS}} = (\mathrm{vTEC_{GNSS}}(t), t = 1, \ldots, n)$, where $\mathrm{vTEC_{GNSS}}(t)$ (UQRG products) is a value at a discrete time t and n is the number of data points in the time series, and we will forecast the $\mathrm{vTEC_{GNSS}}(t+1)$ at time $t+1$. The actual input data to the model are the volatility index [23],

$$r(t) = \log \frac{\mathrm{vTEC_{GNSS}}(t+1)}{\mathrm{vTEC_{GNSS}}(t)} \quad (1)$$

The volatility index is used to determine the abrupt local changes in the $\mathrm{vTEC_{GNSS}}$ series. The benefit of using the volatility index instead of vTEC data is that reduces adverse effects of possible linear trends on the predictions [24].

2.3 Artificial neural networks

Artificial neural networks (ANNs) have been used in a wide range of fields, such as pattern recognition, prediction, grouping, optimization, among others. Generally, ANNs are structured as three layers: input layer, hidden layer(s) and output layer. The hidden layer connects the input and output layers via several nodes, weights, biases and activation functions. All the parameters defining the ANNs need to be estimated on a training phase in which the output of the ANNs to the training data is known. In

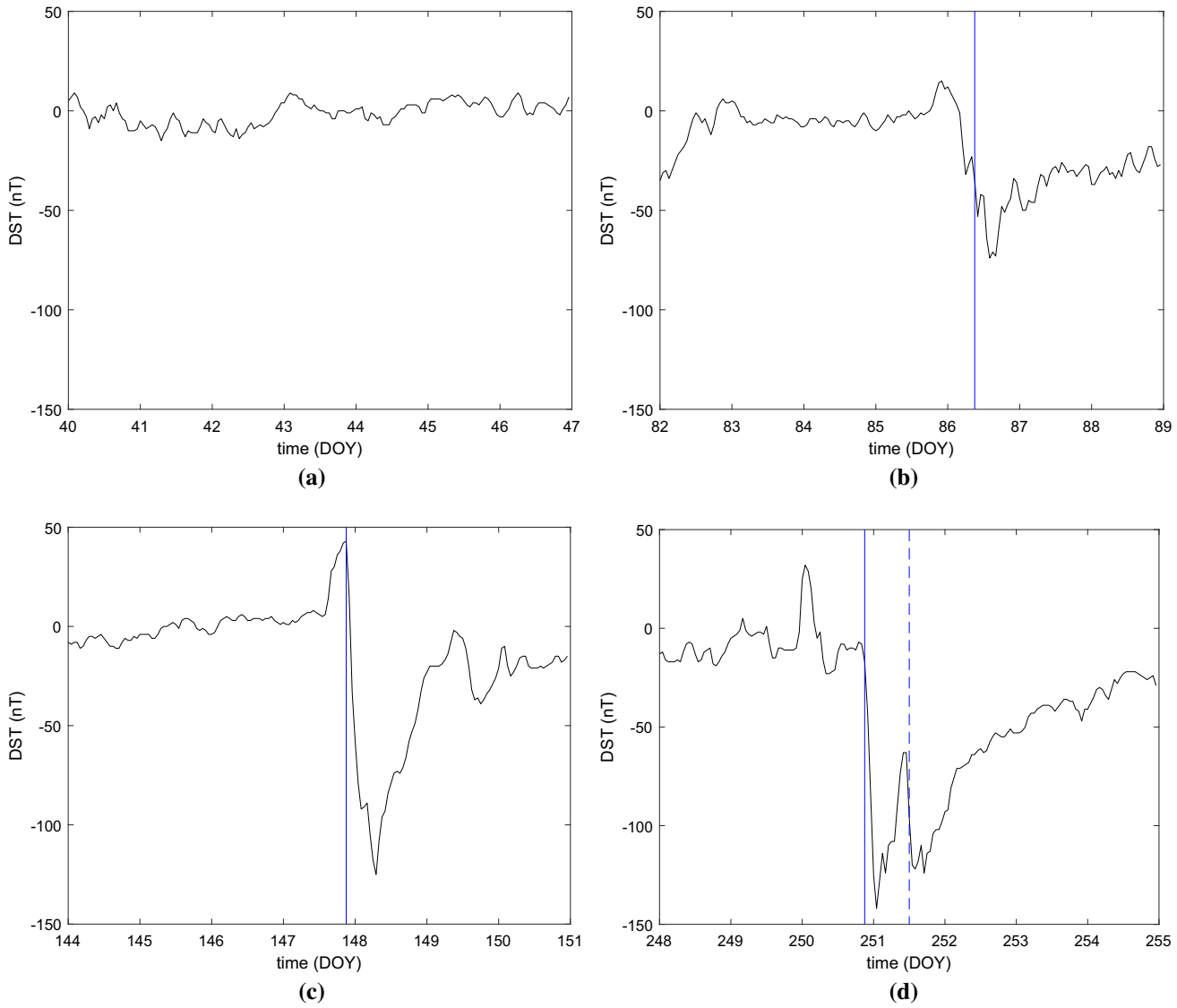

Fig. 2 DST values for periods P1 (**a**), P2 (**b**), P3 (**c**) and P4 (**d**). Vertical lines in **b**–**d** show the Storm Start Time described in Table 2

this work, the corresponding training data sets for P1, P2, P3 and P4 weeks involved time series spanning several weeks in advance.

In this study, we analyze the performance of two different ANNs: ANFIS and NAR. A brief description of both models is presented. More details about both ANNs could be found in [25, 26].

2.3.1 The adaptive neuro-fuzzy inference system (ANFIS)

ANFIS has been shown to be powerful in modeling numerous processes such as hydrological time series modeling [27], permeability prediction [28], time series prediction [29] among others, showing powerful qualities for the modeling and prediction of time series with nonlinear tendencies.

The ANFIS is an adaptive network-based fuzzy inference system that is based on Takagi–Sugeno fuzzy inference system. The ANFIS combines the learning capability of neural networks with the capability of fuzzy logic. The fuzzy inference system is a rule-based system consisting of three conceptual components. These are (1) a rule base, containing fuzzy if-then rules (2) a database, defining the membership function and (3) an inference system, combining the fuzzy rules and producing the system results [30].

More details on adaptive networks have been presented by [31, 32].

Table 3 Results of using training period lengths of 90, 60 and 30 days for period P3

	TUCU			LPGS			RIO2			OHI2		
	30 prev	60 prev	90 prev	30 prev	60 prev	90 prev	30 prev	60 prev	90 prev	30 prev	60 prev	90 prev
ANFIS												
MAE	0.26	0.01	0.007	0.09	0.08	0.09	0.003	0.03	0.003	0.03	0.01	0.03
MAPE	15.85%	15.26%	15.25%	11.72%	11.61%	11.91%	11.68%	10.84%	10.99%	9.21%	7.83%	7.85%
RMSE	2.01	1.69	1.67	1.21	1.14	1.14	0.62	0.59	0.60	0.62	0.43	0.46
NRMSE	0.38	0.30	0.31	0.37	0.34	0.25	0.49	0.48	0.49	0.64	0.46	0.48
NAR												
MAE	0.19	0.01	0.008	0.04	0.06	0.07	0.009	0.03	0.01	0.01	0.01	0.01
MAPE	15.35%	14.81%	14.90%	11.02%	11.14%	11.31%	11.13%	10.98%	10.93%	7.66%	7.74%	7.54%
RMSE	1.79	1.58	1.57	1.08	1.05	1.05	0.61	0.59	0.60	0.41	0.42	0.41
NRMSE	0.32	0.37	0.31	0.33	0.29	0.32	0.48	0.45	0.43	0.43	0.41	0.40

In order to create a model comparable to the NAR-NN structure (which is explained in the next section), the ANFIS model is set up using the volatility series, and the training pattern has been composed as follows:

$$\{\boldsymbol{r(t-3)} \quad \boldsymbol{r(t-2)} \quad \boldsymbol{r(t-1)} \quad \rightarrow \quad \boldsymbol{r(t)}\} \tag{2}$$

This training pattern has three input and one output variables, that is, the three previous elements in the time series are used to forecast the next element.

ANFIS network consists of three input variables and one output variable, i.e., the previous three elements in the volatility time series are used to predict the next element (see Eq. 2). Each input variable is represented by a fuzzy membership function. The generalized Bell was used in this study with two fuzzy rules. In the ANFIS training process for the $r(t)$, forecasting is completed when one of the following conditions is reached: that the difference between the output obtained in the network and the desired output be equal to the error established a priori, or by completing the number of epochs, also pre-established. When one of the above conditions has been reached, ANFIS completes the training and generates an output file, corresponding to the inference of $r(t)$.

2.3.2 Nonlinear autoregressive neural network (NAR-NN)

A nonlinear autoregressive neural network, applied to time series forecasting, describes a discrete, nonlinear, autoregressive model that can be written as follows [33]:

$$r(t) = h(r(t-1), r(t-2), ..., r(t-p)) \tag{3}$$

This equation shows how the NAR-NN is used to predict the values of a time series r using the p past values of the series. The function $h(\cdot)$ is unknown in advance, and the training of the neural networks aims to approximate the function by means of the optimization of the network weights and neuron bias. The p features $r(t-1), r(t-2), \ldots, r(t-p)$, are called feedback delays. The number of hidden layers and neurons per layer are completely flexible and are optimized through a trial-and-error procedure to obtain the network structure that can provide the best performance. The Levenberg–Marquardt backpropagation (LMBP) was used as the learning rule and the hyperbolic tangent sigmoid transfer function for the neurons of intermediate layers.

Both ANNs described imply the use of some common procedures. The optimum training time series length and sampling rate must be defined through testing.

Finally, the predicted volatility must be transformed back to TEC units as follows:

$$\mathrm{vTEC}_f(t+1) = \exp(r(t)).\mathrm{vTEC}_{\mathrm{GNSS}}(t) \tag{4}$$

where vTEC_f corresponds to the forecasted vTEC.

3 Results

The main goal of this work is to set up a neural network-based strategy for real-time vTEC prediction. In order to test two possible approaches, we have selected four different geomagnetic locations on 4 1-week periods having a variety of geomagnetic disturbance levels. This ensures a representative set of forecast conditions are covered. In all tests, the neural network training interval (T) was a continuous series preceding each epoch selected for vTEC prediction. The effect of using training period lengths of 90, 60 and 30 days was investigated. In addition, the prediction system response was evaluated for 60 and 30 min sampling rate vTEC time series. Both NN implementations were trained with 70% of the data in T. The remaining data were used to validate (15%) and test (15%).

Table 4 Statistics for the $vTEC_f$ forecast using the ANFIS and the NAR-NN model during the periods P1 to P4 with 60 min sampling

	ANFIS model				NAR-NN model			
	MAE	MAPE	RMSE	NRMSE	MAE	MAPE	RMSE	NRMSE
P1								
TUCU	0.15	9.64	1.97	0.23	0.16	9.24	1.80	0.21
LPGS	0.17	9.32	1.52	0.23	0.11	8.72	1.43	0.22
RIO2	0.04	5.66	0.97	0.50	0.01	5.70	0.97	0.50
OHI2	0.04	5.01	0.78	0.40	0.03	4.92	0.77	0.39
P2								
TUCU	0.41	20.90	3.27	0.28	0.50	18.81	3.03	0.26
LPGS	0.34	12.73	1.94	0.23	0.38	11.73	1.78	0.21
RIO2	0.13	10.80	1.58	0.56	0.11	10.37	1.48	0.53
OHI2	0.07	8.82	0.88	0.49	0.07	8.63	0.88	0.48
P3								
TUCU	0.26	15.85	2.01	0.38	0.19	15.35	1.79	0.32
LPGS	0.09	11.72	1.21	0.37	0.04	11.02	1.08	0.33
RIO2	0.003	11.68	0.62	0.49	0.009	11.13	0.61	0.48
OHI2	0.03	9.21	0.62	0.64	0.01	7.66	0.41	0.43
P4								
TUCU	0.16	18.49	3.56	0.38	0.30	18.23	3.42	0.36
LPGS	0.36	18.32	2.73	0.42	0.23	15.59	2.24	0.34
RIO2	0.07	10.47	1.05	0.38	0.08	9.98	1.01	0.36
OHI2	0.04	11.01	0.99	1.01	0.03	9.34	0.78	0.35

In the NAR-NN case for each parameter test, every epoch was predicted 100 times. From the 100 outcomes, the mean and median values were computed. This analysis showed that the value of the median over the 100 outcomes is the closest to the $vTEC_{GNSS}$ value. Therefore, NAR-NN predicted values for every epoch are based on the median value. For ANFIS case, this methodology is not applied because of how the network is defined.

To evaluate forecasting accuracy, five of the more popular direct error measures are mean squared error (MSE), or its variants such as root mean squared error (RMSE) and normalized root mean square error (NRMSE), mean absolute error (MAE) and mean absolute percentage error (MAPE)

$$\mathrm{MSE} = \frac{\sum_{i=1}^{n}(\mathrm{vTEC}_{\mathrm{GNSS}} - \mathrm{vTEC}_f)^2}{n} \tag{5}$$

$$\mathrm{RMSE} = \sqrt{\mathrm{MSE}} \tag{6}$$

$$\sigma = \sqrt{\frac{\sum_{i=1}^{n}(\mathrm{vTEC}_{\mathrm{GNSS}} - \overline{\mathrm{vTEC}_{\mathrm{GNSS}}})^2}{n-1}} \tag{7}$$

$$\mathrm{NRMSE} = \frac{1}{\sigma}\mathrm{RMSE} \tag{8}$$

$$\mathrm{AE} = |\mathrm{vTEC}_f - \mathrm{vTEC}_{\mathrm{GNSS}}| \tag{9}$$

$$\mathrm{MAE} = \frac{\sum_{i=1}^{n}\mathrm{AE}_i}{n} \tag{10}$$

$$\mathrm{APE} = \frac{\mathrm{AE}}{\mathrm{vTEC}_{\mathrm{GNSS}}} \tag{11}$$

$$\mathrm{MAPE} = \frac{\sum_{i=1}^{n}\mathrm{APE}_i}{n} * 100 \tag{12}$$

where AE (Eq. 9) represents the absolute error and APE (Eq. 11) represents the absolute relative error for one epoch, being $vTEC_f$ the forecasted value obtained from each model and n is the number of epochs predicted. According to Lewis [34], MAPE values of less than 10% indicate that the method gives a highly accurate forecast, values in the range between 10 and 20% indicate a good forecast, between 20 and 50% a reasonable forecast, while values over 50% indicate an inaccurate forecast.

Table 3 shows how the NN behaves when different T training intervals are used. The results did not show a significant improvement when T is longer although it takes more computation time. Thus, a training period length of 30 days was used.

To analyze the results, it is important to briefly describe how vTEC behaves under different conditions. This parameter shows variations in space (e.g., with geomagnetic location: polar, aurora zones, mid-latitudes and equatorial regions) and time (sunspot cycle, seasonal and diurnal). In particular, ionospheric storms represent an

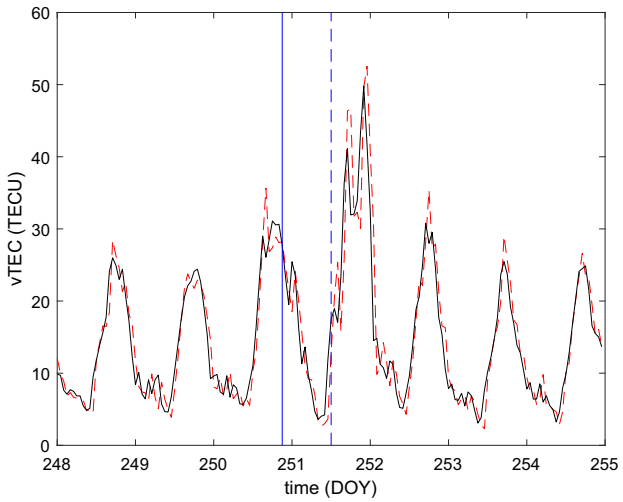

(a) ANFIS model

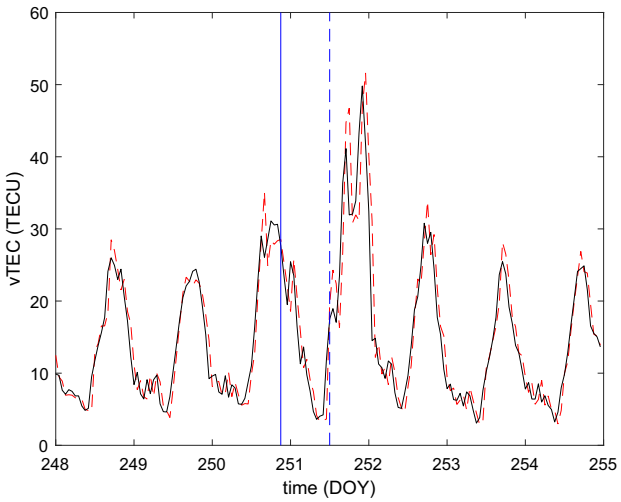

(b) NAR-NN model

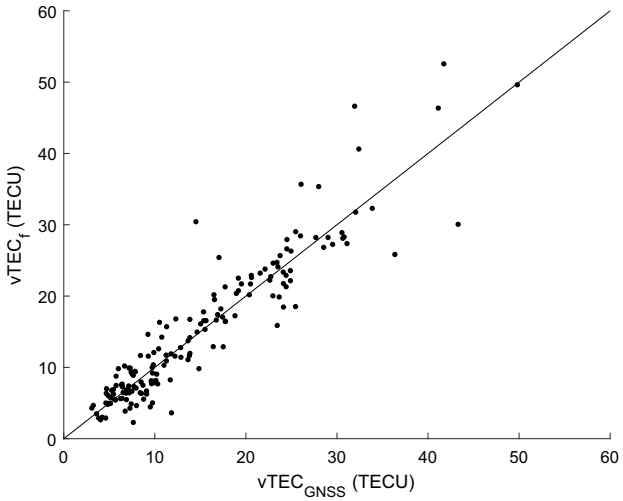

(c) ANFIS model

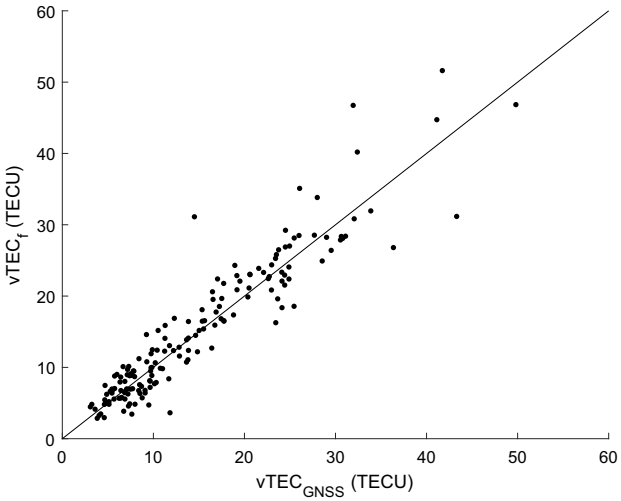

(d) NAR-NN model

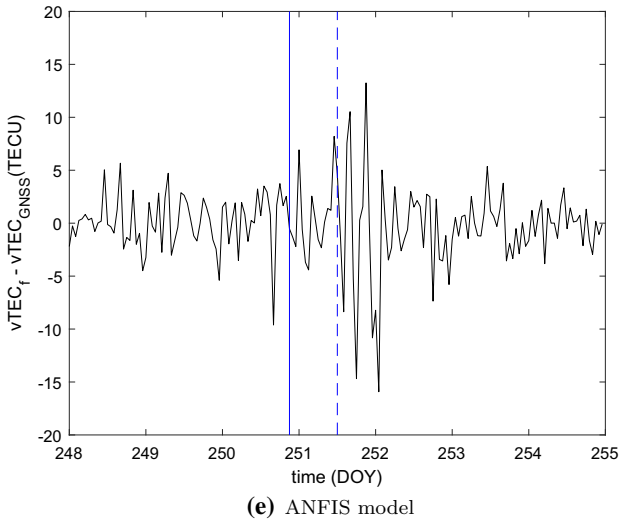

(e) ANFIS model

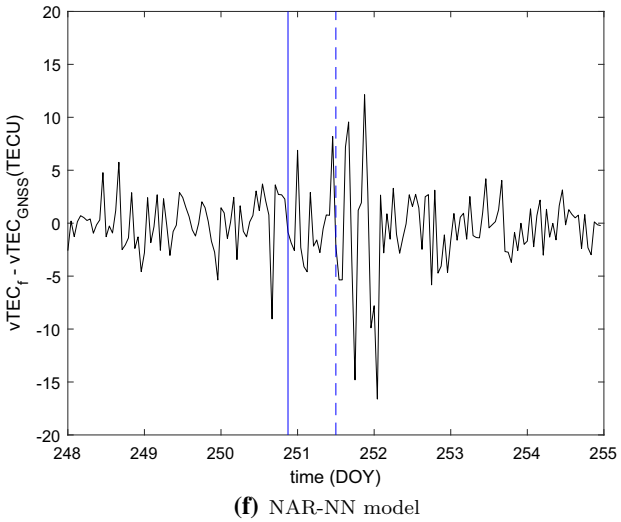

(f) NAR-NN model

◀**Fig. 3** **a**, **b** Show $vTEC_{GNSS}$ (solid black line) and the forecasted $vTEC_f$ (dashed red line) applying the ANFIS and the NAR-NN models, respectively, with 60 min sampling for P4; **c**, **d** show the scatter plots of the $vTEC_{GNSS}$ values versus $vTEC_f$ values; **e**, **f** are the residuals between $vTEC_f$ and the $vTEC_{GNSS}$. Vertical lines in **a**–**d** show the Storm Start Time described in Table 2 (color figure online)

extreme form of space weather with important effects on ground- and space-based technological systems. Consequently, the values of vTEC show both an anomalous increase as well an anomalous decrease over the course of magnetic storm. According to [35], negative storm effect is due to changes in the neutral composition and initiated always in the post-midnight sector and rotated with the Earth into forenoon sector; therefore, they affect the ionosphere of station located in the post-midnight and morning sectors. The positive storm effect can be divided into the daytime and the nighttime manifestation. The former case is expected attributed to traveling atmospheric disturbance [36], most often seen in the afternoon and evening sector. The positive storm at nighttime [37] is initiated before dusk and [38] suggested that if this kind of storm was driven by winds before dusk, it would rotate into the night side.

At this point, it is important to stress that this work does not intend to analyze geomagnetic storms in detailed, we selected perturbed periods only to test the efficiency of our models to predict vTEC values under different conditions.

First, a comparison between both NNs, ANFIS and NAR-NN, in order to select the model which better represent vTEC time series, is presented. Then, the sampling rate was reduced from 60 to 30 min to test the NN response.

3.1 Comparison between ANFIS and NAR-NN models

Several authors have proposed different statistical methods such as multiple regression approaches, like autocorrelation and neural networks to forecast ionospheric parameters. Most forecasting methods were developed to predict classical ionospheric parameters such as $f0F2$ and $MUF(3000)F2$. Kutiev et al. [39] presented an autocorrelation method (ACM) to predict $f0F2$ for some ionospheric stations. They evaluated their results using the prediction efficiency parameter which is based on the standard deviations of the prediction and input data. They found a clear dependence of the prediction quality on the latitude of the station, being better for mid-geomagnetic latitude than for high latitudes. Later, Muhtarov et al. [40] improved ACM through the addition of the cross-correlation between $f0F2$ and a geomagnetic index. This was termed geomagnetically correlated autoregression model (GCAM).

Table 5 Statistics for the $vTEC_f$ forecast comparing two different sampling frequency: 60 min and 30 min, using the NAR-NN model during the periods P1 to P4

	60 min				30 min			
	MAE	MAPE	RMSE	NRMSE	MAE	MAPE	RMSE	NRMSE
P1								
TUCU	0.16	9.24	1.80	0.21	0.03	5.78	1.07	0.12
LPGS	0.11	8.72	1.43	0.22	0.02	4.89	0.90	0.14
RIO2	0.01	5.70	0.97	0.50	0.01	3.65	0.61	0.31
OHI2	0.03	4.92	0.77	0.39	0.001	3.59	0.56	0.29
P2								
TUCU	0.50	18.81	3.03	0.26	0.24	10.21	1.93	0.17
LPGS	0.38	11.73	1.78	0.21	0.12	6.46	1.09	0.13
RIO2	0.11	10.37	1.48	0.53	0.01	6.80	0.87	0.31
OHI2	0.07	8.63	0.88	0.48	0.01	5.13	0.51	0.28
P3								
TUCU	0.19	15.35	1.79	0.32	0.03	10.03	1.06	0.19
LPGS	0.04	11.02	1.08	0.33	0.02	6.35	0.60	0.18
RIO2	0.009	11.13	0.61	0.48	0.01	7.19	0.41	0.33
OHI2	0.01	7.66	0.41	0.43	0.002	4.49	0.24	0.26
P4								
TUCU	0.30	18.23	3.42	0.36	0.14	10.80	2.05	0.22
LPGS	0.23	15.59	2.24	0.34	0.07	10.92	1.22	0.18
RIO2	0.08	9.98	1.01	0.36	0.05	6.67	0.66	0.24
OHI2	0.03	9.34	0.78	1.01	0.02	5.90	0.49	0.22

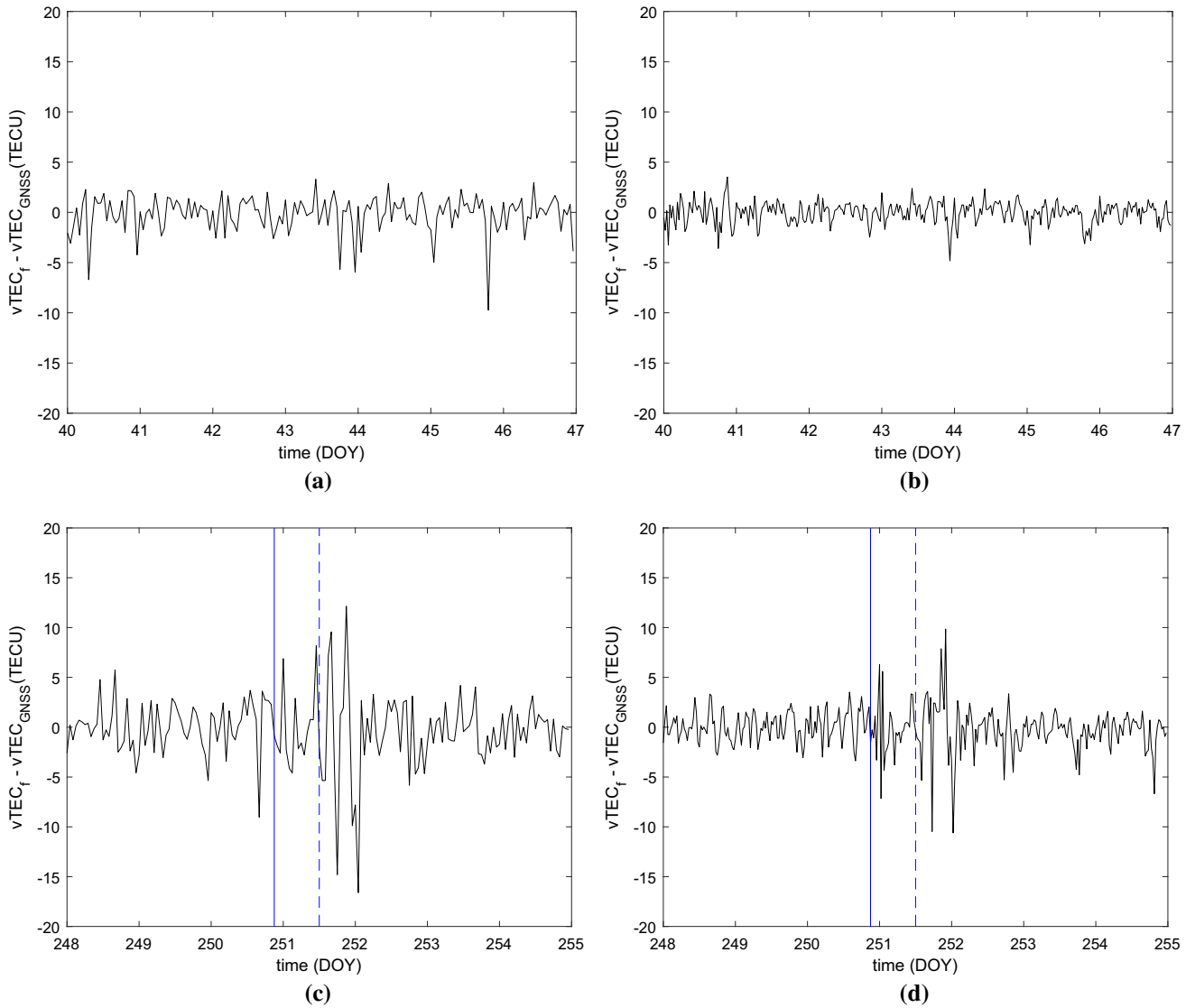

Fig. 4 **a**, **b** Shows the residuals between the $vTEC_f$ and the $vTEC_{GNSS}$ using 60 and 30 min sampling for P1; **c**, **d** idem to **a**, **b** for P4. Vertical lines in **c**, **d** shows the Storm Start Time described in Table 2

Cander [41] compared GCAM technique with a neural network-based autoregressive model with additional inputs (NNARX). The *f*0*F*2 forecast periods chosen in this study correspond to quiet and disturbed geomagnetic conditions from mid-latitude ionosonde measurements. Both techniques indicated a very good result over the geomagnetically quiet period, but NNARX showed a better performance over the severe storm period.

In this section, we will describe some results from different authors who worked in TEC forecast applying NNs and how they compare to ours.

Table 4 shows the performance for each period and both NNs. For P1 period, the mean absolute error is almost zero for all stations and both NNs. MAPE value presents a different behavior for the two NNs and the four stations under analysis. MAPE values decrease when the geomagnetic latitude increases and the NAR model shows a slightly better performance than ANFIS. This behavior shows that both NNs during a quiet period are more efficient to represent the values of vTEC over stations at high than at low geomagnetic latitude, where the ionosphere is more complicated to predict. σ also confirm this result and show a better performance using NAR-NN model.

For P1, a quiet period (Fig. 2a and Table 2), MAPE took values near 10%, being smaller for high latitudes. P2, P3 and P4 are disturbed periods containing geomagnetic storms with different characteristics. Particularly, the storm that occurs in P3 (Fig. 2c) is classified as intense according

to its DST value [42] with all the classical development phases described in the literature [35, 43]. In this case, a MAPE up to 15% was obtained for low latitudes and near 10% for mid- and high latitudes. P2 contains a geomagnetic storm classified as moderate (Fig. 2b and Table 2). MAPE is 11% and 8% for mid- and high latitudes, respectively, which are similar to results obtained for P3. In the case of low latitude, MAPE reaches 21% which is significantly higher than the corresponding value for P3. Thus, P2 is more difficult to represent than P3 for low latitudes. To explain this, it is important to mention not only the magnitude of the geomagnetic storm but also the local time when the perturbation is developed: 11 a.m. for P2 and 4 a.m. for P3 as shown on Table 2. As mentioned in Sect. 3, others authors characterized the complexity of the vTEC behavior depending on the local time of storm development. P4 is the period with the greatest disturbance. It contains the succession of two storms (Fig. 2d and Table 2). Table 2 shows that MAPE does not exceed 18.5% for low- and mid-latitudes, nor 10% for high latitudes.

As an example of the results obtained, Fig. 3 shows the behavior of the $vTEC_{GNSS}$ (solid black line) and the $vTEC_f$ (dashed red line) for P4 for both NNs. Table 2 and Fig. 2 contain the evolution of the two intense geomagnetic storms that take place in that period. The first one occurs at local sunset hours and during the recovery period a new storm begins around 9 LT, reaching its maximum at local noon. Scatter plots (Fig. 3c, d) show a good agreement that corresponds with a correlation coefficient of 0.95. Figure 3e, f shows the residuals for both NNs which do not show significant systematics. At the end of DOY 251 (2017-09-07) and the beginning of DOY 252 (2017-09-08), the residuals reach extreme values of + 12 to − 16 TECU. This period corresponds to the development of both storms. For the days before and after the perturbations, residuals take values between ± 5 TECU.

Tulunay et al. [19] developed METU-NN using GPS measurements to predict TEC. The analysis was performed over mid-high geomagnetic latitudes between November 16 and 29 of 2003, including a geomagnetic storm. The RMSE values at mid-high latitudes are between 2.15 and 2.05 TECU, and MAPE took values between 14 and 16%. They also analyzed the performance of the network during the day where the storm takes place obtaining values between 20 and 27%. Our results showed MAPE values between 10 and 12 % for RIO2 (the only station at mid-high latitude) when the three perturbed periods are considered. If we isolate the perturbed day, MAPE values of 13%, 17% and 15 % are obtained for RIO2 for P2, P3 and P4 periods, respectively, showing a better performance than Tulunay's forecast. We can also highlight the results obtained by [44]. She presented a 1 hr ahead TEC forecast using a hybrid time-delay multilayer perceptron (MLP) [45]. The period tested corresponds to the ten quietest (10 Q-days) and five disturbed (5 D-days) days (http://wdc.kugi.kyoto-u.ac.jp/qddays) during December 1990 for one mid-latitude station. The performance of the neural network proved to be quite accurate with a MAPE of 13.57%, while our results show an improvement between 20 and 25% (see Table 4, RIO2).

We can conclude that both NN models show highly accurate and good forecast according to [34] classification, although the NAR-NN model shows slightly better results. This improvement is up to 3% in terms of MAPE and can be seen on Table 2 periods analyzed.

3.2 30 and 60 min sampling NAR-NN vTEC forecast

The prediction quality sensitivity of the NAR-NN to different sampling rates of the input vtec time series was analyzed. Table 5 shows the results for all four periods analyzed for the cases of 60 and 30 min sampled input vTEC. The values of MAPE are significantly lower if the forecast is made to predict values every 30 min. The improvement observed is between 27 and 47%. This behavior is evident for all four periods analyzed and can also be seen in the vTEC residuals as shown in Fig. 4 for TUCU station on P1 and P4 datasets, representing quiet and highly perturbed conditions, respectively. Indeed, Fig. 4b, d, shows that for 30 min sampling rate, the residuals are consistently smaller except in the close vicinity of extremely anomalous events associated with the storms where they peak in a much more isolated way that in the case of the 60 min sampling experiment.

4 Conclusions

The applicability of the adaptive neuro-fuzzy inference system and nonlinear autoregressive neural network in forecasting the vertical total electron content variability is presented in this paper. The ANFIS and the NAR-NN are networks with different internal structures, and we have applied the same input and output structure to make a comparison between both models. We have selected four different geomagnetic locations on 4 1-week periods having a variety of geomagnetic disturbance levels. The effect of using training period lengths of 90, 60 and 30 days was investigated. In addition, the prediction system response was evaluated for 60 and 30 min sampling rate vTEC time series. The main conclusions are:

1. Both NN's models learned the shape of the inherent nonlinearities.

2. MAPE differences of .5% where find using different training period's lengths, based on this result 30 days training periods were used;
3. The higher MAPE values are during geomagnetic storms; reaching values up to 20% for ANFIS and 18% for NAR-NN;
4. Highly accurate and good forecast were obtained according to [34] classification;
5. NAR-NN model shows a slightly better performance than ANFIS, this difference is up to 3%;
6. When the NAR-NN model forecasts values for 30 min in advance, the results improve considerably, and the MAPE is reduced up to 47% compared to MAPE when 60 min sampling rate is used.
7. Our future work is to use this methodology to forecast vTEC values on a grid over the Argentina region.

Acknowledgements This research was supported by ANPCyT Grant PICT 2015-3710 and UNLP Grant 11/G142. The authors thank the International GNSS Service (ftp://cddis.gsfc.nasa.gov) for providing the IONEX data and to the NASA/GSFC's Space Physics Data Facility's OMNIWeb Plus Service. Finally, we thank the two anonymous reviewers for their insightful comments on the original manuscript.

Compliance with ethical standards

Conflict of interest The authors declare that there are no conflict of interest regarding this manuscript.

References

1. Bothmer V, Daglis IA (2007) Space weather: physics and effects. Springer, Berlin
2. Schrijver CJ, Kauristie K, Aylward AD, Denardini CM, Gibson SE, Glover A, Gopalswamy N, Grande M, Hapgood M, Heynderickx D et al (2015) Understanding space weather to shield society: a global road map for 2015–2025 commissioned by COSPAR and ILWS. Adv Space Res 55(12):2745–2807
3. Tsagouri I, Koutroumbas K, Elias P (2018) A new short-term forecasting model for the total electron content storm time disturbances. J Space Weather Space Clim 8:A33
4. Gao ZG, Zhang LQ (2006) Multi-seasonal spectral characteristics analysis of coastal salt marsh vegetation in Shanghai, China. Estuar Coast Shelf Sci 69(1–2):217–224
5. Le A, Tiberius C, van der Marel H, Jakowski N (2009) Use of global and regional ionosphere maps for single-frequency precise point positioning. In: Sideris MG (ed) Observing our changing earth. International Association of Geodesy Symposia, vol 133. Springer, Berlin, Heidelberg, pp 759–769
6. Meehan J, Fisher G, Murtagh W (2010) Understanding space weather customers in GPS-reliant industries. Space Weather 8(6):1–3
7. Board, Space Studies and National Research Council and others (2009) Severe space weather events: understanding societal and economic impacts: a workshop report. National Academies Press
8. Bust GS, Mitchell CN (2008) History, current state, and future directions of ionospheric imaging. Rev Geophys 46(1):RG1003
9. Dow JM, Neilan RE, Rizos C (2009) The international GNSS service in a changing landscape of global navigation satellite systems. J Geod 83(3–4):191–198
10. Hernandez-Pajares M, Juan JM, Sanz J, Orus R, Garcia-Rigo A, Feltens J, Komjathy A, Schaer SC, Krankowski A (2009) The IGS VTEC maps: a reliable source of ionospheric information since 1998. J Geod 83(3–4):263–275
11. Garcia-Rigo A, Monte E, Hernandez-Pajares M, Juan JM, Sanz J, Aragon-Angel A, Salazar D (2011) Global prediction of the vertical total electron content of the ionosphere based on GPS data. Radio Sci 46(06):1–3
12. Erdogan E, Schmidt M, Seitz F, Durmaz M (2017) Near real-time estimation of ionosphere vertical total electron content from GNSS satellites using B-splines in a Kalman filter. Ann Geophys 35(2):263–277
13. Jakowski N, Mayer C, Hoque MM, Wilken V (2011) Total electron content models and their use in ionosphere monitoring. Radio Sci 46(6):1–11
14. Takahashi H, Wrasse CM, Denardini CM, Pádua MB, Paula ER, Costa SMA, Otsuka Y, Shiokawa K, Monico JF, Ivo A et al (2016) Ionospheric TEC weather map over South America. Space Weather 14(11):937–949
15. Mendoza LPO, Meza AM, Paz JMA (2019) A multi-GNSS, multi-frequency and near real-time ionospheric TEC monitoring system for South America. Space Weather 17(5):654–661
16. Badeke R, Borries C, Hoque MM, Minkwitz D (2018) Empirical forecast of quiet time ionospheric Total Electron Content maps over Europe. Adv Space Res 61(12):2881–2890
17. Williscroft L-A, Poole AWV (1996) Neural networks, foF2, sunspot number and magnetic activity. Geophys Res Lett 23(24):3659–3662
18. Wintoft P, Cander LR (2000) Twenty-four hour predictions of f0F2 using time delay neural networks. Radio Sci 35(2):395–408
19. Tulunay E, Senalp ET, Radicella SM, Tulunay Y (2006) Forecasting total electron content maps by neural network technique. Radio Sci 41(4):1–12
20. Tebabal A, Radicella SM, Nigussie M, Damtie B, Nava B, Yizengaw E (2018) Local TEC modelling and forecasting using neural networks. J Atmos Sol Terr Phys 172:143–151
21. Mallika IL, Ratnam DV, Ostuka Y, Sivavaraprasad G, Raman S (2019) Implementation of hybrid ionospheric TEC forecasting algorithm using PCA-NN method. IEEE J Sel Top Appl Earth Obs Remote Sens 12(1):317–381
22. Orus R, Hernandez-Pajares M, Juan JM, Sanz J (2005) Improvement of global ionospheric VTEC maps by using kriging interpolation technique. J Atmos Sol Terr Phys 67(16):1598–1609
23. Popoola A, Ahmad S, Ahmad K (2004) A fuzzy-wavelet method for analyzing non-stationary time series. In: Proceedings of the 5th international conference on recent advances in soft computing, pp 16–18
24. Akyilmaz O, Arslan N (2008) An experiment of predicting Total Electron Content (TEC) by fuzzy inference systems. Earth Planets Space 60(9):967–972
25. Takagi T, Sugeno M (2008) Fuzzy identification of systems and its applications to modeling and control. IEEE Trans Syst Man Cybern 15(1):116–132
26. Isasi Vinuela P, Galvan Leon IM (2004) Redes de neuronas artificiales. Editorial Pearson Educacion SA, Madrid
27. Mahmut F, Mahmud G (2008) Hydrological time-series modelling using an adaptive neuro-fuzzy inference system. Hydrol Process Int J 22(13):2122–2132
28. Nuri H, Milagrosa A, Julio T (2009) Comparison between neuro-fuzzy and fractal models for permeability prediction. Comput Geosci 13(2):181–186

29. Melin P, Soto J, Castillo O, Soria J (2012) A new approach for time series prediction using ensembles of ANFIS models. Expert Syst Appl 39(3):3494–3506
30. Walia N, Singh H, Sharma A (2015) ANFIS: adaptive neuro-fuzzy inference system a survey. Int J Comput Appl 123(13):32–38
31. Brown M, Harris CJ (1994) Neurofuzzy adaptive modelling and control. Prentice Hall, Upper Saddle River
32. Jang J-SR (1993) ANFIS: adaptive-network-based fuzzy inference system. IEEE Trans Syst Man Cybern 23(3):665–685
33. Ruiz L, Cuellar M, Calvo-Flores M, Jimenez M (2016) An application of non-linear autoregressive neural networks to predict energy consumption in public buildings. Energies 9(9):684
34. Lewis CD (1982) Industrial and business forecasting methods: a practical guide to exponential smoothing and curve fitting. Butterworth-Heinemann, Oxford
35. Prölss G (2012) Physics of the earth's space environment: an introduction. Springer, Berlin
36. Tsagouri I, Belehaki A, Moraitis G, Mavromichalaki H (2000) Positive and negative ionospheric disturbances at middle latitudes during geomagnetic storms. Geophys Res Lett 27(21):3579–3582
37. Belehaki A, Tsagouri I (2001) Study of the thermospheric-ionospheric response to intense geomagnetic storms at middle latitudes. Phys Chem Earth Part C Sol Terr Planet Sci 26(5):353–357
38. Fuller-Rowell TJ, Codrescu MV, Moffett RJ, Quegan S (1994) Response of the thermosphere and ionosphere to geomagnetic storms. J Geophys Res Space Phys 99(A3):3893–3914
39. Kutiev I, Muhtarov P, Cander LR, Levy MF (1999) Short-term prediction of ionospheric parameters based on auto-correlation analysis. Ann Geophys 42(1):121–127
40. Muhtarov P, Kutiev I, Cander L (2002) Geomagnetically correlated autoregression model for short-term prediction of ionospheric parameters. Inverse Probl 18(1):49
41. Cander LR (2015) Forecasting foF2 and MUF (3000) F2 ionospheric characteristics—a challenging space weather frontier. Adv Space Res 56(9):1973–1981
42. Gonzalez WD, Jo-Ann J, Kamide Y, Kroehl HW, Rostoker G, Tsurutani BT, Vasyliunas VM (1994) What is a geomagnetic storm? J Geophys Res Space Phys 99(A4):5771–5792
43. Hargreaves JK (1992) The solar-terrestrial environment: an introduction to geospace-the science of the terrestrial upper atmosphere, ionosphere, and magnetosphere. Cambridge University Press, Cambridge
44. Cander LR (2019) Ionospheric space weather forecasting and modelling. In: Ionospheric space weather, pp 135–178
45. Haykin S, Thomson DJ (1998) Signal detection in a nonstationary environment reformulated as an adaptive pattern classification problem. Proc IEEE 89(11):2325–2344